Carcinogenesis, 2023, **44**, 291–303
https://doi.org/10.1093/carcin/bgad020
Advance access publication 13 April 2023
Original Article

Original Article

Inhibition of lung adenocarcinoma by combinations of sulfasalazine (SAS) and disulfiram-copper (DSF-Cu) in cell line models and mice

Alireza Jian Bagherpoor[1], Mohammad Shameem[1], Xianghua Luo[1,2], Davis Seelig[1,3] and Fekadu Kassie[1,3,*]

[1]Masonic Cancer Center, Minneapolis, MN 55455, USA
[2]Division of Biostatistics, School of Public Health, Minneapolis, MN 55455, USA
[3]College of Veterinary Medicine, University of Minnesota, Saint Paul, MN 55108, USA
*Corresponding author: Tel: +1 612 625 9637Email: kassi012@umn.edu

Abstract

Sulfasalazine (SAS) is a repurposed antitumor drug which inhibits the proliferation and survival of cancer cells by inhibiting the xCT cellular antioxidant system. Recent clinical studies have shown that, due to poor bioavailability, the antitumor effects of SAS monotherapy are minimal. Therefore, we hypothesized that DSF, another repurposed drug that has demonstrated anticancer effects, or its complex with copper (DSF-copper, DSF-Cu) could potentiate the antilung cancer effects of SAS. Exposure of non-small cell lung cancer cells to therapeutically achievable concentrations of SAS-induced low-to-moderate cytotoxic effects (20–40% reduction in cell viability) and, unexpectedly, induced the antioxidant protein NRF2 and its downstream effectors xCT and ALDH1A1. However, combinations of SAS and DSF-Cu, but not SAS and DSF, induced a significantly higher cytotoxic effect (64–88% reduction in cell viability), apoptosis and generation of mitochondrial reactive oxygen species as compared with SAS or DSF-Cu alone. Moreover, DSF-Cu abrogated SAS-induced NRF2, xCT and ALDH1A1 expression. In a mouse model of lung tumor, SAS + DSF-Cu showed a higher efficacy than the individual drugs in reducing the number and size of tumors as well as the incidence and multiplicity of lung adenocarcinoma. Taken together, our findings indicate that the observed antilung cancer effects of SAS plus DSF-Cu are mediated, at least in part, via impairment of reactive oxygen species defense and enhancement of oxidative stress and provide evidence for the preventive/therapeutic potential of this combinatorial approach against lung cancer.

Received: December 27, 2022; Revised: March 20 2023; Accepted: April 11, 2023

Graphical Abstract

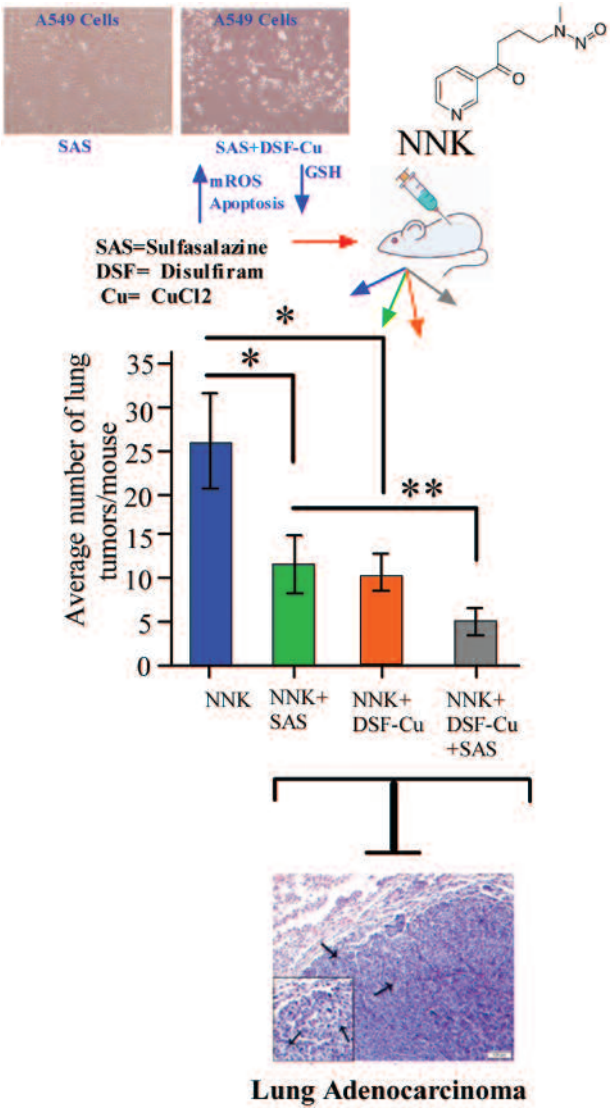

Abbreviations: DSF-Cu, disulfiram-copper; mROS, mitochondrial reactive oxygen species; NSCLC, non-small cell lung cancer; SAS, sulfasalazine.

Introduction

Lung cancer is the leading cause of cancer-associated death in the USA (1). The American Cancer Society estimated that 236 740 new cases of lung cancer would be diagnosed in the USA by the end of 2022, and there would be 130 180 lung cancer-related deaths, accounting for ~21% of all cancer deaths. Although recent advances in cancer biology have led to the development of novel-targeted therapies and improvement in the survival of lung cancer patients, in males, mortality from lung cancer is still more than colorectal and prostate cancer mortalities combined (1).

The most frequent oncogenic mutation among patients with non-small cell lung cancer (NSCLC), which represents about 80–85% of lung cancer cases in western countries, is mutation in *KRAS* (2). In recent years, it has become widely appreciated that oncogenic KRAS signaling influences intracellular redox balance to drive malignant transformation (3–5) via increased transcriptional induction of *xCT* (*Slc7a11*). xCT, the functional light chain subunit of the cystine/glutamate antiporter system x_c^-, is a major rate-limiting factor in glutathione biosynthesis (6) and is essential for RAS-induced tumorigenicity (5,7).

Sulfasalazine (SAS) is a drug originally approved by FDA for the treatment of ulcerative colitis or rheumatoid arthritis, but later found to be a potent inhibitor of xCT and repurposed as an antitumor drug (8,9). In particular, SAS has been found to inhibit the proliferation of drug-resistant cancer cells and cancer stem-like cells via inhibition of xCT-mediated glutathione synthesis and induction of oxidative stress (10). However, recent clinical studies in patients with lung cancer (11), gastric cancer (12) and glioma (13) have shown that the antitumor efficacy of SAS monotherapy is minimal, probably as a result of poor bioavailability (11). Moreover, SAS has been shown to induce reactive oxygen species (ROS)-dependent nuclear translocation and activation of nuclear factor erythroid-2-related factor 2 (Nrf2) (14), which though recognized originally as suppressor of early-stage carcinogenesis by regulating multiple downstream cytoprotective genes, now established as a driver of cancer progression, metastasis and resistance to therapy (15). One promising approach to enhance the anticancer effects of SAS could be co-administration with disulfiram (DSF), an FDA-approved drug that has been clinically used for the treatment of alcoholism for almost 70

years (16) and has demonstrated, alone or in combination with copper (DSF-Cu), anticancer effects in several models, at least in part, via induction of oxidative stress (16–18) and inhibition of NRF2 (19,20).

In the present study, we observed that SAS-induced cytotoxic effects in several NSCLC cell lines differing in their genetic background in a dose-dependent manner. However, strong effects (>50% reduction in cell viability) were induced only at concentrations that are unlikely to be achieved at target tissues in lung cancer patients. Moreover, NSCLC cells treated with SAS, in particular at lower concentrations, exhibited upregulation of NRF2 as a compensatory mechanism to maintain redox homeostasis. Combinations of low concentrations of SAS and DSF-Cu, compared with SAS alone, not only resulted in higher killing effects in NSCLC cells but also enhanced mitochondrial ROS (mROS) levels and the percentage of apoptotic cells, reduced glutathione levels and abrogated SAS-induced NRF2 upregulation. In a mouse lung tumor bioassay, we assessed the efficacy of SAS and DSF/DSF-Cu, alone or in combination, to inhibit malignant progression of lung tumors induced by 4-(methylnitrosamino)-1-(3-pyridyl)-1-butanone (NNK), a tobacco-specific carcinogen considered to be carcinogenic to humans (21) and induces lung tumors with a high proportion of mutations in the *K-ras* oncogene (22). SAS, DSF-Cu and SAS plus DSF-Cu markedly and significantly reduced the multiplicity and size of tumors on the surface of the lung as well as multiplicities and incidence of lung adenocarcinoma and the strongest effects were induced in mice treated with SAS plus DSF-Cu. Overall, our findings indicate that enhancing ROS generation using combinations of SAS and DSF-Cu is a promising approach for the prevention and therapy of lung cancer.

Materials and methods

Cell lines and chemicals

NSCLC cell lines H522, H2030, A549 and H1975 were purchased from ATCC. The authenticity of the cells was determined by short tandem repeat analysis technology at MD Anderson's Cell Line Core Facility. We routinely carry out mycoplasma screening for all of our cell lines. All cell lines were tested for mycoplasma infection and authenticated by short tandem repeat method at MD Anderson's Cell Line Core Facility in February 2020. All NSCLC cell lines were cultured in RPMI 1640 medium supplemented with 10% fetal bovine serum in 5% CO_2 incubator at 37°C. SAS and copper were purchased from Sigma–Aldrich (St. Louis, MO); DSF was from Combi-Blocks (San Diego, CA). NNK was purchased from Toronto Research Chemicals, Toronto, Canada. Anti-NRF2, anti-ALDH1A1, anti-xCT, anti-phospho-Akt (Ser 478), anti-total Akt, anti-phospho-ERK (T202/Y204), anti-total ERK, anti-GAPDH, anti-β-actin and goat anti-rabbit IgG secondary antibody were from Cell Signaling Technology (Beverly, MA). Anti-poly (ADP-ribose) polymerase (PARP) was obtained from Santa Cruz Biotechnology.

Cell viability assay

The effects of SAS and/or DSF/DSF-Cu on the viability of NSCLC cells were determined by methylthiazole tetrazolium (MTT; Biotium, Hayward, CA) assay as described previously (23). Potential synergy between SAS and DSF or SAS and DSF-Cu was determined by calculating synergy scores using the Bliss independence model (24). Synergy scores of <–10, –10 to 10 and >10 indicate antagonism, additive effects and synergistic effects, respectively.

Annexin V/propidium iodide apoptosis assay

To determine the apoptotic effects of SAS and/or DSF-Cu in NSCLC cells, each cell line was treated with different concentrations of the drugs for 24. Subsequently, 1 × 10^6 cells were washed twice with cold phosphate-buffered saline and stained with 5 µl annexin V-fluorescein isothiocyanate and 5 µl propidium iodide (BD Pharmingen, San Diego, CA) for 15 min at room temperature in the dark. The proportion of apoptotic cells was determined by BD LSRII flow cytometer.

Detection of mROS levels using flow cytometry

After 24 h of exposure to SAS, DSF, DSF-Cu, SAS + DSF or SAS + DSF-Cu, A549 and H2030 cells were stained with MitoSOX Red Mitochondrial Superoxide Indicator (Thermo Fisher Scientific) for the detection of mROS. A working concentration of 5 µM mitoSOX Red was used, and cells were incubated at 37°C for 10 min. After washing off excess dye, cells were trypsinized and analyzed by flow cytometry.

Measurement of intracellular GSH levels

Total GSH and GSSG (oxidized glutathione) in A549 and H2030 cells were measured by Glutathione Colorimetric Detection Kit (Invitrogen, MA) following the recommendation of the manufacturer. Total GSH content was calculated from a standard curve created from a 250 µM GSH standard supplied by the manufacturer. The free GSH concentration in samples was calculated by subtracting the GSSG content from the total GSH.

Western blot analysis of NSCLC cells

For the preparation of lysates from cell cultures, DMSO- or drug-treated NSCLC cells were incubated in 1× RIPA buffer with protease inhibitor and phosphatase inhibitor (Pierce, Rockford, IL) for 10 min on ice. Subsequently, cell lysates were centrifuged at 14 000*g* for 10 min at 4°C, the supernatants collected, aliquoted and stored at −80°C. Western immunoblotting analysis of the different proteins was performed as we reported previously (25). For each protein, at least three western blot assays were carried out. To quantify protein levels, densitometric measurements of western blot bands were performed using digitalized scientific software program UN-SCAN-IT software (Silk Scientific, Orem, UT).

Assessment of the lung tumor inhibitory effects of SAS, DSF and DSF-Cu, alone or in combination, in A/J mice

The mouse tumor bioassay was performed as we described previously (26) following the guidance of the Institutional Animal Care and Use Committee. Briefly, 6-week-old female A/J mice (Jackson Laboratory, Bar Harbor, ME) were randomized into seven groups (10 mice for group 1 and 15 mice each for the remaining groups) and received physiological saline solution as vehicle control (group 1) or two doses of NNK (groups 2–7). From 20 weeks after the first carcinogen dose, the time lung adenoma develops in NNK-treated mice (26), until the end of the study at week 45, mice in groups 3–7 were given SAS (250 mg/kg) (27), DSF (100 mg/kg) (28), DSF-Cu (DSF, 100 mg/kg, Cu, 2 mg/kg), SAS + DSF or SAS + DSF-Cu

every other day (3 times/week) by oral gavage. Following the allometric scaling of Reagan-Shaw *et al.* (29), the dose of SAS used in the present study amounts to a human equivalent dose of 20 mg/kg or 1.2 g/person (for a person with a body weight of 60 kg). This dose of SAS is less than the dose of SAS (1.5 g) administered in a phase I clinical trial and found to be safe (11). Similarly, the doses of DSF (100 mg/kg) and $CuCl_2$ (2 mg/kg) given to the mice amount to 486 and 9.7 mg/person, respectively. A dose level of 500 mg DSF/person was found to be well tolerated when given to glioblastoma patients (30) and the acceptable upper level of copper in humans is 8–10 mg/day (31).

Body weights were measured weekly throughout the study. At the end of week 45, mice were euthanized with an overdose of carbon dioxide and the lungs were harvested, and the number and size of tumors on the surface of the lung determined under a dissecting microscope. Lungs from 5 mice/group/assay were preserved in 10% buffered formalin for subsequent histopathology and immunohistochemistry (IHC) studies, whereas the remaining lungs were kept in liquid nitrogen and stored at −80°C for western immunoblotting studies.

Histopathological analysis of lung tumors

Formalin-fixed lung tissues were processed through a series of graded alcohols, embedded in paraffin and three step sections (each 200 µm apart) having a thickness of 4 µm were cut and stained with hematoxylin and eosin. Proliferative lesions were counted and classified, at each step section, as atypical adenomatous hyperplasia, adenoma, adenoma with dysplasia, adenoma with progression or adenocarcinoma according to our previous reports (32) and the recommendations of the Mouse Models of Human Cancer Consortium (33).

Statistical analyses

Between group comparisons were performed using one-way analysis of variance followed by Dunnett's multiple comparisons procedure to determine differences among the treatments. *P* values <0.05 were considered and all analyses were conducted in SAS 9.4.

Results

Combinatory cytotoxic effects of SAS and DSF-Cu in NSCLC cells

To determine the cytotoxicity of SAS in NSCLC cells, A549, H2030, H522 and H1975 cells differing widely in their molecular alterations, were exposed to the drug for 48 h and cell viability was analyzed by MTT assay. H522 cells were the most sensitive of all NSCLC cells to the cytotoxicity of SAS and the viability of these cells was reduced by about 80% at 400 µM (Figure 1A). However, for all other cell lines, more than 400 µM of SAS were required to reduce the viability of cells by 50%. These concentrations of SAS are unlikely to be achieved at target tissues (11) or could lead to dose-limiting toxicities (13). Therefore, we postulated that combinations of SAS with DSF or DSF-Cu could potentiate the anticancer effects of low concentrations of SAS. Before assessing the combinatory effects of SAS and DSF/DSF-Cu, we examined the cytotoxic effects of low concentrations of DSF and DSF-Cu. At the range of concentrations tested, neither DSF (250, 400 or 500 nM), nor DSF-Cu (250 nM DSF plus 250 or 500 nM of Cu or 500 nM DSF plus 250 nM Cu), reduced the viability of NSCLC cells by more than 50% although the effects, compared with the effects of the vehicle control (DMSO), were significant. Also, the cytotoxicity of combinations of SAS (300 µM) and DSF (400 nM) was not significantly different from the effects of the individual drugs. On the other hand, compared with SAS alone (300 µM) or DSF-Cu alone (250 nM DSF plus 500 nM of Cu and 500 nM DSF plus 250 nM Cu), their combinations significantly reduced the viability of A549, H522, H2030 and H1975 cells at least by about 50% (Figure 1B). Assessment of potential synergism, using Bliss synergy score analysis which assumes independence between the combined drugs, indicated that the interaction between SAS and DSF-Cu was clearly synergistic (Bliss synergy score of 36.5, Supplementary Figure 1, available at *Carcinogenesis* Online).

Cell death induced by SAS plus DSF-Cu is mediated mainly via apoptosis

To determine the mode of cell death induced by SAS, DSF-Cu and their combinations in NSCLC cells, A549 and H2030 cells were exposed to the drugs for 24 h and apoptotic cell death was assessed by flow cytometry-based annexin V/propidium iodide assay. Compared with vehicle (DMSO)-treated A549 and H2030 cells, SAS- or DSF-treated cells exhibited a non-significant and slight but significant increase, respectively, in the percentage of apoptotic cells, whereas DSF-Cu significantly and markedly increased these effects (Figure 2A and B). As compared with cells treated with DSF-Cu only, combinations of SAS and DSF-Cu significantly increased the proportion of apoptotic cells. Furthermore, exposure of H2030 cells to SAS plus DSF-Cu for a longer time (48 h) dramatically increased (up to 70%) the percentage of apoptotic cells (Supplementary Figure 2, available at *Carcinogenesis* Online).

Combinatory treatment with SAS and DSF-Cu enhanced mROS levels in A549 and H2030 cells

mROS are a major determinant of both mitochondria-dependent and -independent apoptosis (34). To determine if the high rate of apoptosis in SAS plus DSF-Cu-treated A549 and H2030 cells will be paralleled by an increase in mROS levels, cells were stained with MitoSOX Red Mitochondrial Superoxide Indicator (Thermo Fisher Scientific) and the level of mROS was determined by flow cytometry. mROS generation by SAS, DSF, DSF-Cu or SAS + DSF-Cu in A549 and H2030 cells was, more or less, in line with the efficacy of these drugs to induce apoptosis and SAS + DSF-Cu induced significantly more mROS than DSF-Cu alone (Figure 3A and B). Moreover, mROS levels increased in a manner dependent on the concentration of both DSF and Cu. Overall, these results suggest that the strong apoptotic effects of SAS plus DSF-Cu might be initiated through ROS generation, which subsequently activates downstream signaling pathways leading to reduced cell proliferation and survival.

SAS-induced overexpression of NRF2 and its downstream effectors were abrogated by DSF-Cu

Low levels of ROS activate NRF2, a key transcriptional regulator which protects cells from oxidative DNA damage by inducing the expression of antioxidant genes (35). To determine the effects of low concentrations of SAS on NRF2 and its downstream effectors, A549 cells were treated with the drug for 6, 12, 24 and 48 h and levels of NRF2 and xCT

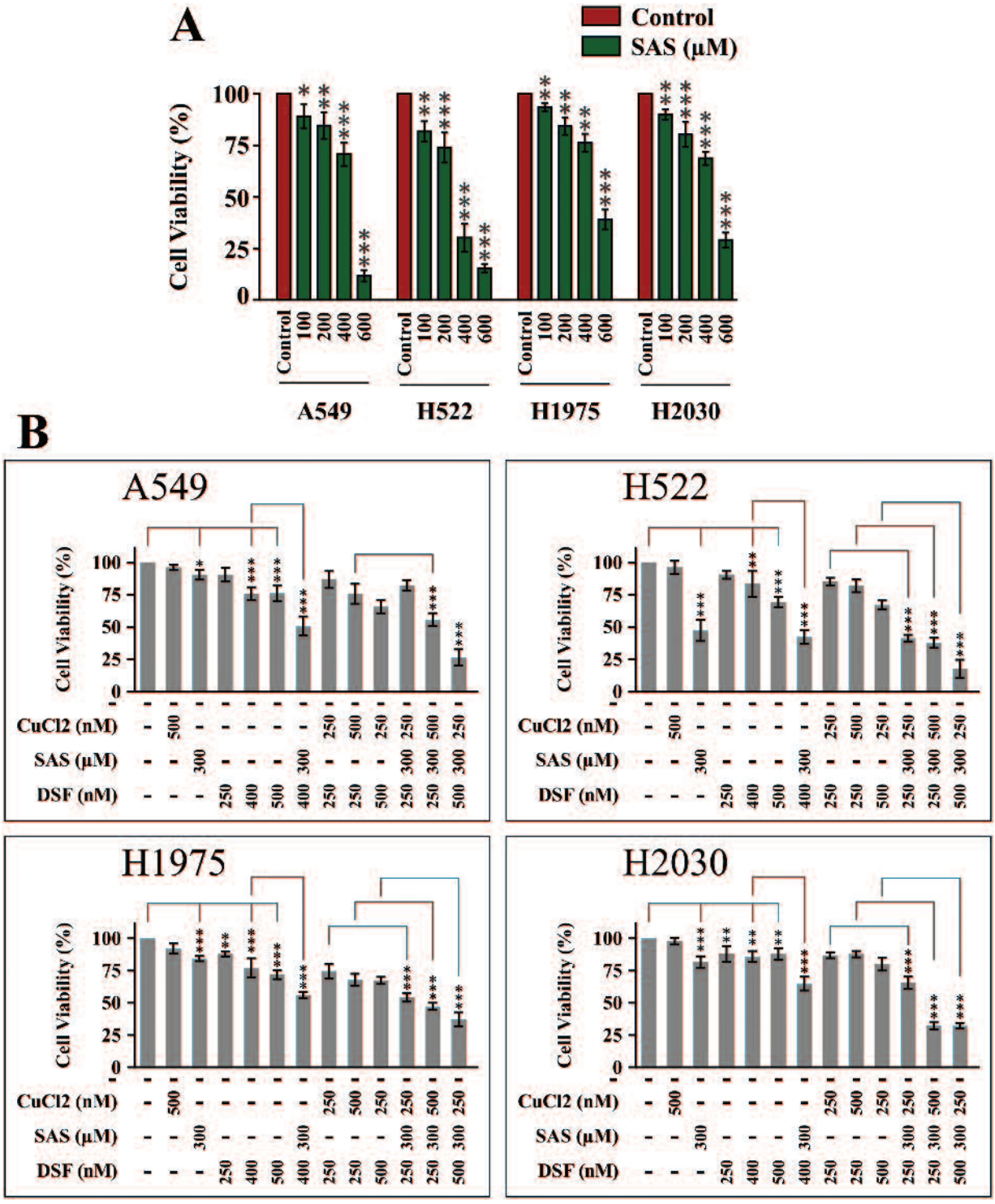

Figure 1. DSF-Cu potentiated the cytotoxic effects of SAS in A549, H522, H2030 and H1975 NSCLC cells. (**A**, **B**) Therapeutically achievable concentrations of SAS (100–300 μM) induced weak to moderate cytotoxicity, as determined by MTT assay, in A549, H2030, H522 and H1975 cells, whereas low concentrations of DSF-Cu potentiated the cytotoxicity of therapeutically achievable concentrations of SAS (300 μM) in these cells. Cells were treated with the drugs in triplicates for 48 h and the assay was performed three times. The bar graphs indicate mean ± SD of the three assays. *$P < 0.05$; **$P < 0.01$; ***$P < 0.001$.

were determined by western immunoblotting. As depicted in Figure 4A and Supplementary Figures 3A and 4A, available at *Carcinogenesis* Online, although the effects of SAS on NRF2 and xCT expression at 6 h is unclear, at later time points (12, 24 and 48 h), there was a marked increase in the level of both NRF2 and xCT and these effects diminished slightly at the higher concentration of SAS (400 μM).

To assess if DSF/DSF-Cu can abrogate induction of NRF2 and its downstream targets by SAS, A549 cells were treated with SAS and DSF/DSF-Cu, alone and in combination, for

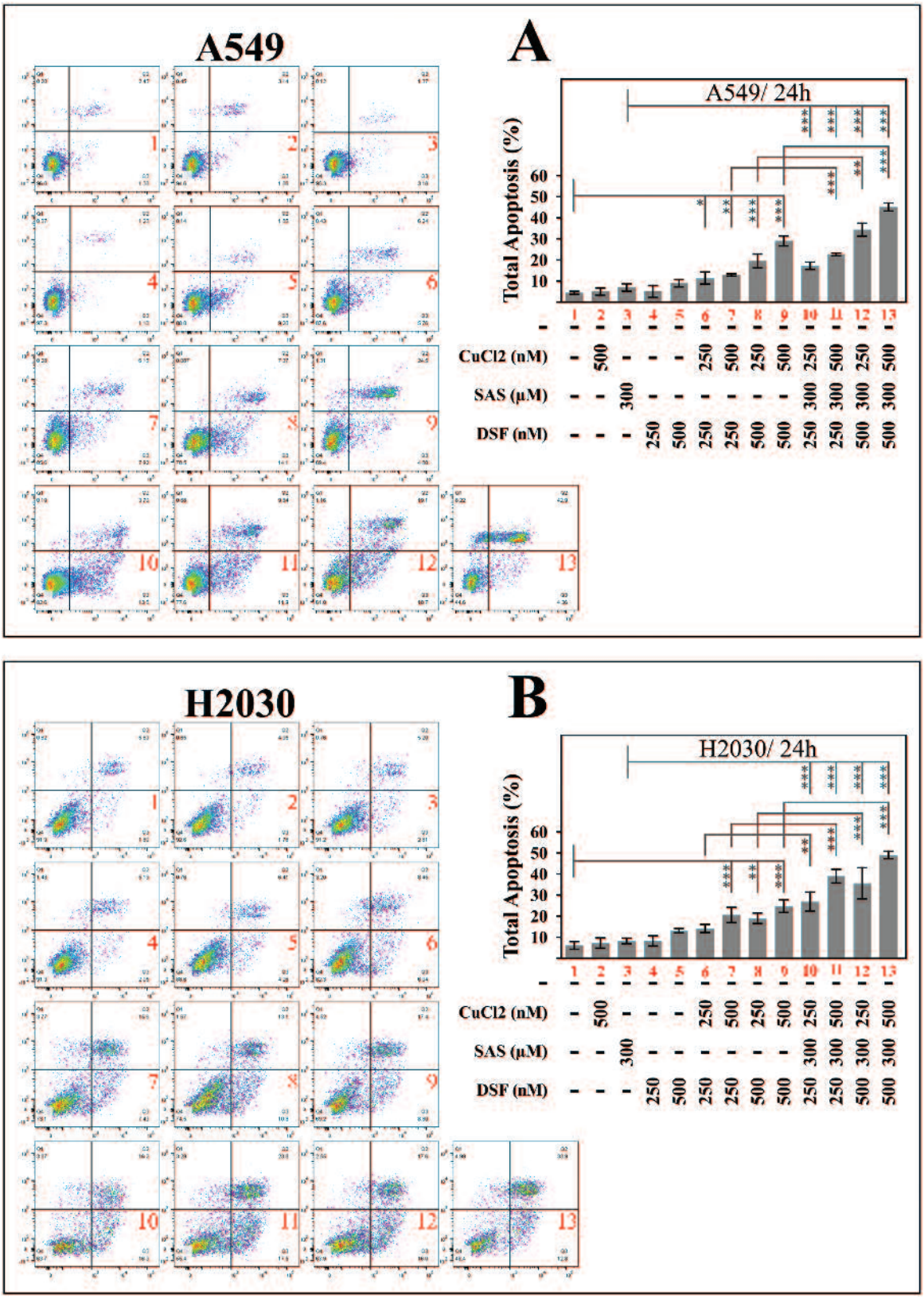

Figure 2. Apoptosis induction in A549 and H2030 cells treated with SAS and/or DSF/DSF-Cu alone or in combination. Representative flow cytometry density plots as well as bar graphs showing mean ± SD of the percentage of apoptotic A549 (**A**) and H2030 (**B**) cells from three assays. Cells were treated with SAS and/or DSF/DSF-Cu, alone or in combination, for 24 h, and analyzed by flow cytometry-based annexin V/propidium iodide assay. *$P < 0.05$; **$P < 0.01$; ***$P < 0.001$.

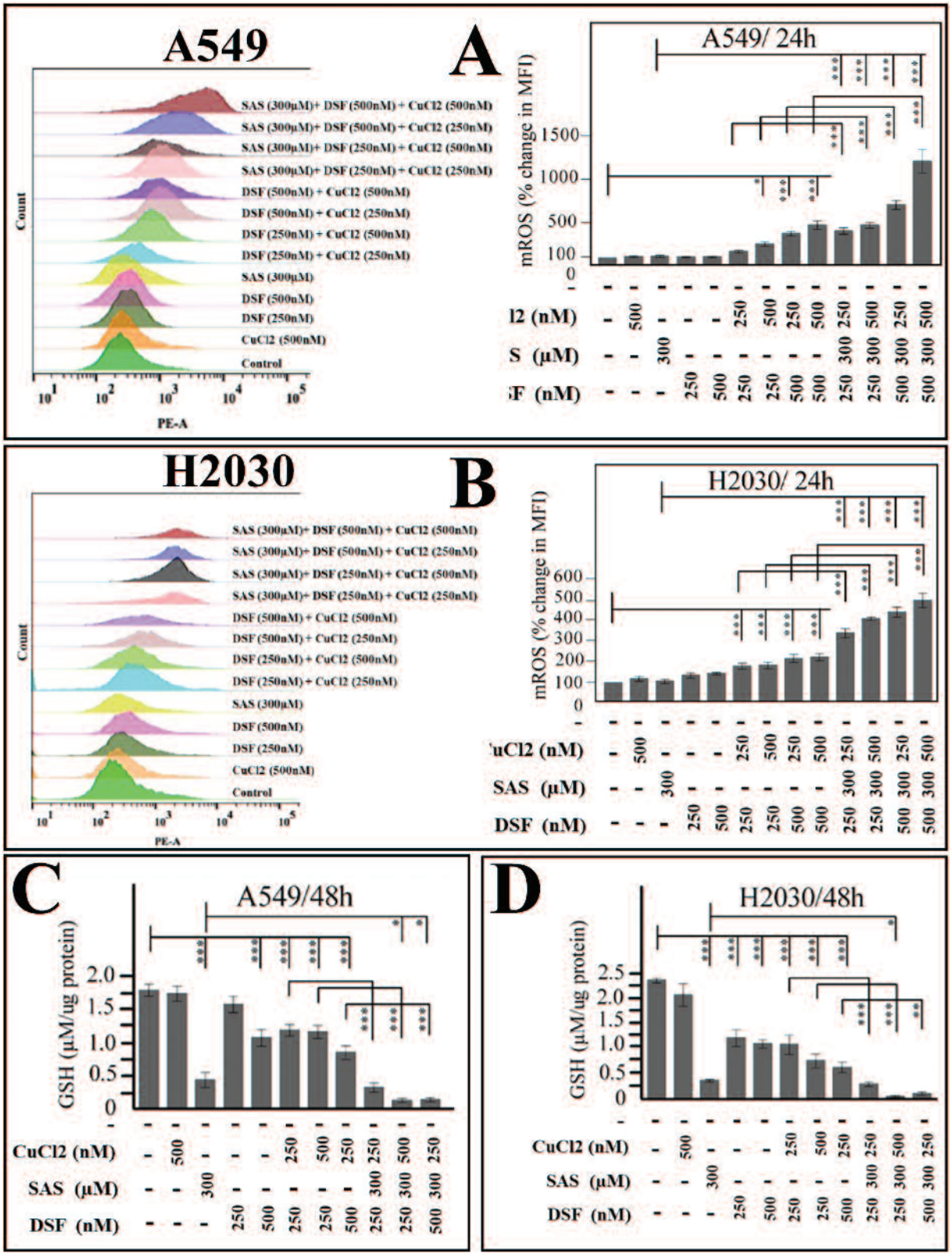

Figure 3. Effects of SAS and/or DSF/DSF-Cu, alone or in combination, on mROS and GSH levels in A549 and H2030 cells. Representative histogram showing mROS levels and bar graphs showing mean ± SD of percentage in MFI in A549 (**A**) and H2030 (**B**) cells from three experiments. Cells were treated with the drugs for 24 h, stained with mitoSOX (mitochondrial ROS) reagent and analyzed by flow cytometry and bar graphs show mean ± SD of data obtained from three independent assays. A549 (**C**) and H2030 (**D**) cells were treated with SAS and/or DSF/DSF-Cu, alone or in combination, 48 h and GSH levels determined as described in Materials and methods. The assay was done in triplicate each time and data represent mean ± SD of results from three independent assays. **P* < 0.05; ***P* < 0.01; ****P* < 0.001.

48 h and the level of NRF2 and its downstream effectors as well as cell proliferation- and survival-related proteins was determined. As expected, compared with vehicle (DMSO)-treated cells, SAS-treated cells exhibited higher level of NRF2, whereas DSF and, in particular, DSF-Cu reduced the level of NRF2 (Figure 4B and Supplementary Figures 3B and 4B, available at *Carcinogenesis* Online). Upon combinatorial treatment, SAS plus DSF-Cu suppressed/abolished the expression of not only NRF2 and its downstream effectors xCT and ALDH1A1, but also reduced the phosphorylation of Akt and ERK and increased PARP cleavage. Next, we assessed the efficacy of DSF-Cu to potentiate silencing of NRF2 and its downstream targets by NRF2 siRNA in A549 cells. NRF2 siRNA markedly reduced the expression of NRF2, its downstream targets xCT and ALDH1A1, as well as phospho-Akt but did not modulate PARP cleavage (Figure 4C and Supplementary Figures 3C and 4C, available at *Carcinogenesis* Online). DSF-Cu clearly enhanced the effects of NRF2 siRNA as indicated by complete abrogation of NRF2, xCT and phospho-Akt, a marked reduction in the level of ALDH1A1 and enhancement of PARP cleavage. Overall, these results indicate that the weak cytotoxicity of SAS toward NSCLC could be attributed to its induction of the cell protective NRF2 antioxidant system and abrogation of these effects by DSF-Cu potentiates the cytotoxicity of SAS.

SAS and DSF/DSF-Cu, alone or in combination, suppressed the multiplicity and size of NNK-induced lung tumors in A/J mice

To further corroborate the antilung cancer activities of SAS and/or DSF/DSF-Cu observed in cell line models, mice pretreated with the tobacco smoke carcinogen NNK were given the drugs (starting 20 weeks after NNK treatment) and the number and size of tumors on the surface of the lung were determined at the end of week 45 (Figure 5A). SAS and/or DSF/DSF-Cu, alone or in combination, had no apparent adverse effects on the mice as determined by body weight measurements (data not shown). The vehicle control group treated with NNK and given vehicle (DMSO + corn oil) exhibited 26 ± 5 lung tumors/mouse, whereas the groups treated with NNK and received SAS, DSF-Cu or SAS + DSF-Cu had 11 ± 3, 10 ± 3 and 5 ± 1 lung tumors/mouse, corresponding to a significant reduction of tumor multiplicity by 58, 62 and 79%, respectively (Figure 5B). Lung tumor multiplicities mice given SAS + DSF-Cu were at least 2-fold lower than those mice given SAS alone or DSF-Cu alone, clearly indicating additive, if not synergistic, antilung tumor effects. Mice treated with NNK and given DSF had 19 ± 4 lung tumors/mouse, which corresponds to a not-significant reduction by 27%. The tumor multiplicities of mice given SAS + DSF (10 ± 4 lung tumors/mouse) were not different from that of mice treated with SAS alone (11 ± 3 lung tumors/mouse), indicating that DSF failed to potentiate the antitumor effects of SAS. Stratification of lung tumors into different size classes indicated that SAS + DSF, DSF-Cu and SAS + DSF-Cu completely abolished the largest lung tumors (>3 mm), whereas SAS and DSF significantly reduced the multiplicity of these tumors (Figure 5C). Moreover, SAS, DSF-Cu, SAS + DSF and SAS + DSF-Cu diminished the number of lung tumors with a size of <1 and 1–3 mm, indicating suppression of the growth of lung tumors.

SAS + DSF-Cu suppressed malignant progression of NNK-induced lung tumors

To determine the effects of SAS and/or DSF-Cu on the multiplicity and incidence of NNK-induced microscopic lung lesions and malignant progression of lung tumors, we assessed the frequency of various microscopic lung lesions, including atypical adenomatous hyperplasia, adenoma (A), adenoma with dysplasia, adenoma with progression and adenocarcinoma. Images of representative lung tissue sections from the different groups of mice as well as the appearance of representative microscopic lesions are depicted in Figure 5D and E, respectively. As shown in Table 1, DSF-Cu, SAS and SAS + DSF-Cu reduced multiplicities of lung adenocarcinoma by 65, 60 and 80%, respectively. Despite the overall strong inhibition of malignant lesions, the effects of SAS on adenocarcinoma did not reach significant levels due to the low incidence of the lesions, the wide intragroup variations in the number of the lesions and the few number of lungs analyzed (5 lungs/group). It is unclear whether the drugs induced the regression of preneoplastic lesions. However, the fact that DSF-Cu, SAS and SAS + DSF-Cu reduced multiplicities of the total number of preneoplastic lesions (atypical adenomatous hyperplasia, adenoma and adenoma with dysplasia or progression) by 31, 50 and 39%, respectively, suggests that the drugs inhibited adenocarcinoma formation, at least in part, via induction of regression in preneoplastic lesions. Overall, SAS and/or DSF-CU inhibited lung adenocarcinoma formation and the strongest effects were observed in mice given SAS + DSF-Cu.

Discussion

Given the high cost and long-time required to develop new anticancer agents, re-purposing of drugs can be a faster and less costly alternative approach (36). In the present study, we assessed the efficacy of two repurposed drugs, SAS and DSF, which were originally developed for the treatment of inflammatory diseases and alcoholism, respectively, against lung cancer. We showed that the cytotoxic effects of maximally achievable therapeutic concentrations of SAS toward NSCLC cells were weak to moderate. However, combinations of low concentrations of SAS and DSF-Cu induced significantly stronger cytotoxic effects, as compared with the effects of SAS or DSF-Cu alone, mainly via mROS-mediated oxidative stress. Furthermore, DSF-Cu reversed SAS-induced overexpression of NRF2 and other antioxidant proteins in NSCLC cells. In a mouse lung tumor bioassay, combinations of SAS and DSF-Cu significantly reduced the multiplicity and size of NNK-induced lung tumors on the surface of the lung as well as the development of premalignant tumors into lung adenocarcinoma.

The major factor limiting the pharmacological effects of SAS and DSF *in vivo* is their poor oral bioavailability resulting in low submicromolar concentrations of the drugs or their active metabolites (37–39). However, published works on the anticancer effects of SAS and DSF have used concentrations at least two orders of magnitude higher than clinically achievable concentrations (9,16,17) and the outcomes of such studies may not be relevant to patients. One potential approach to improve the efficacy of anticancer drugs having low bioavailability is combinatory approach which could open an opportunity not only for maximizing anticancer effects but

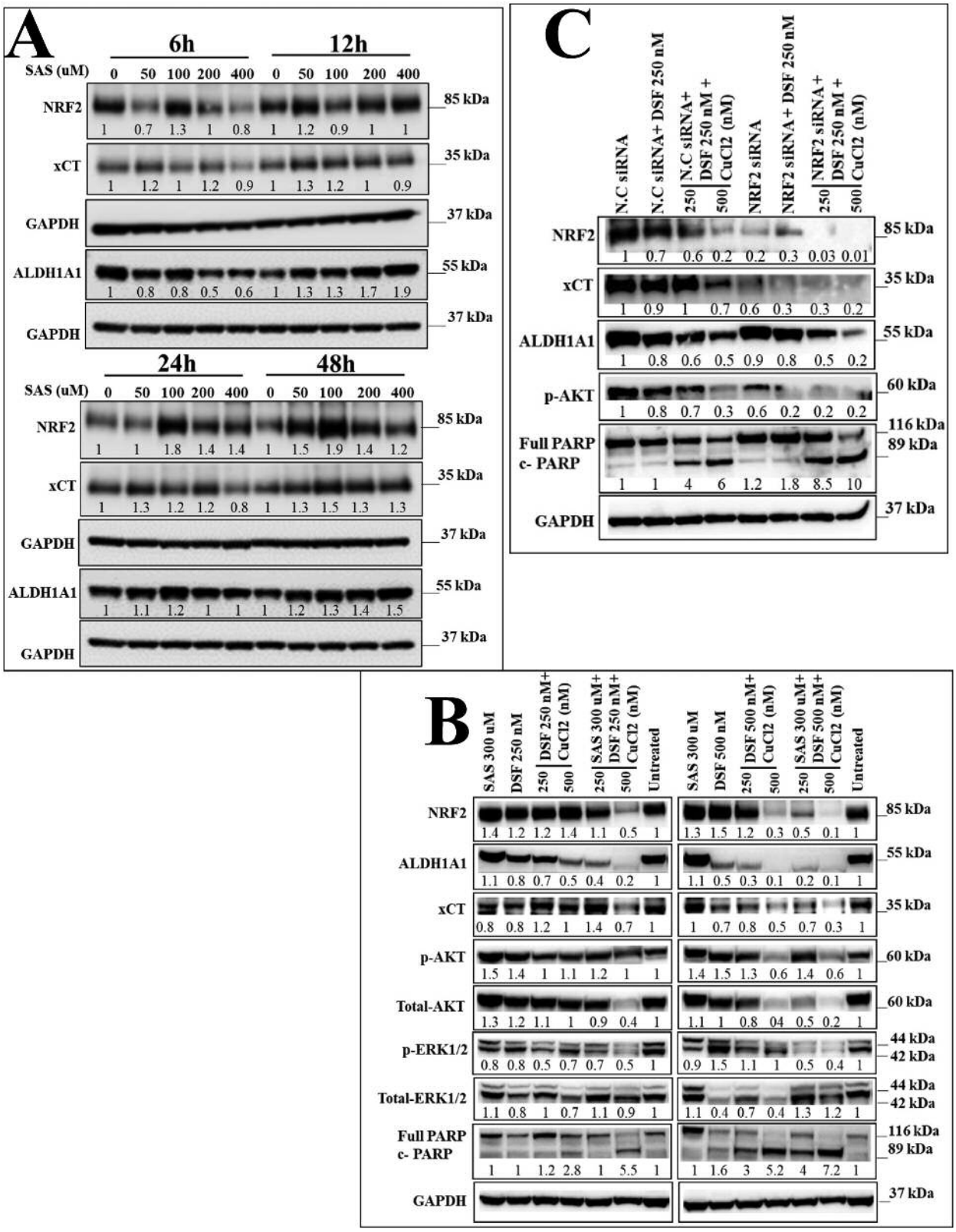

Figure 4. Western blot assays showing (**A**) induction of NRF2, xCT and ALDH1A1 by SAS, (**B**) modulation by DSF-Cu of SAS-induced effects on NRF2, xCT, ALDH1A1 and other proteins and (**C**) modulation by NRF2 siRNA and/or DSF-Cu of levels of xCT, ALDH1A1 and pAkt levels. Western immunoblotting studies were carried at described in Materials and methods and the relative expression of each protein, compared with the level of GAPDH, was shown.

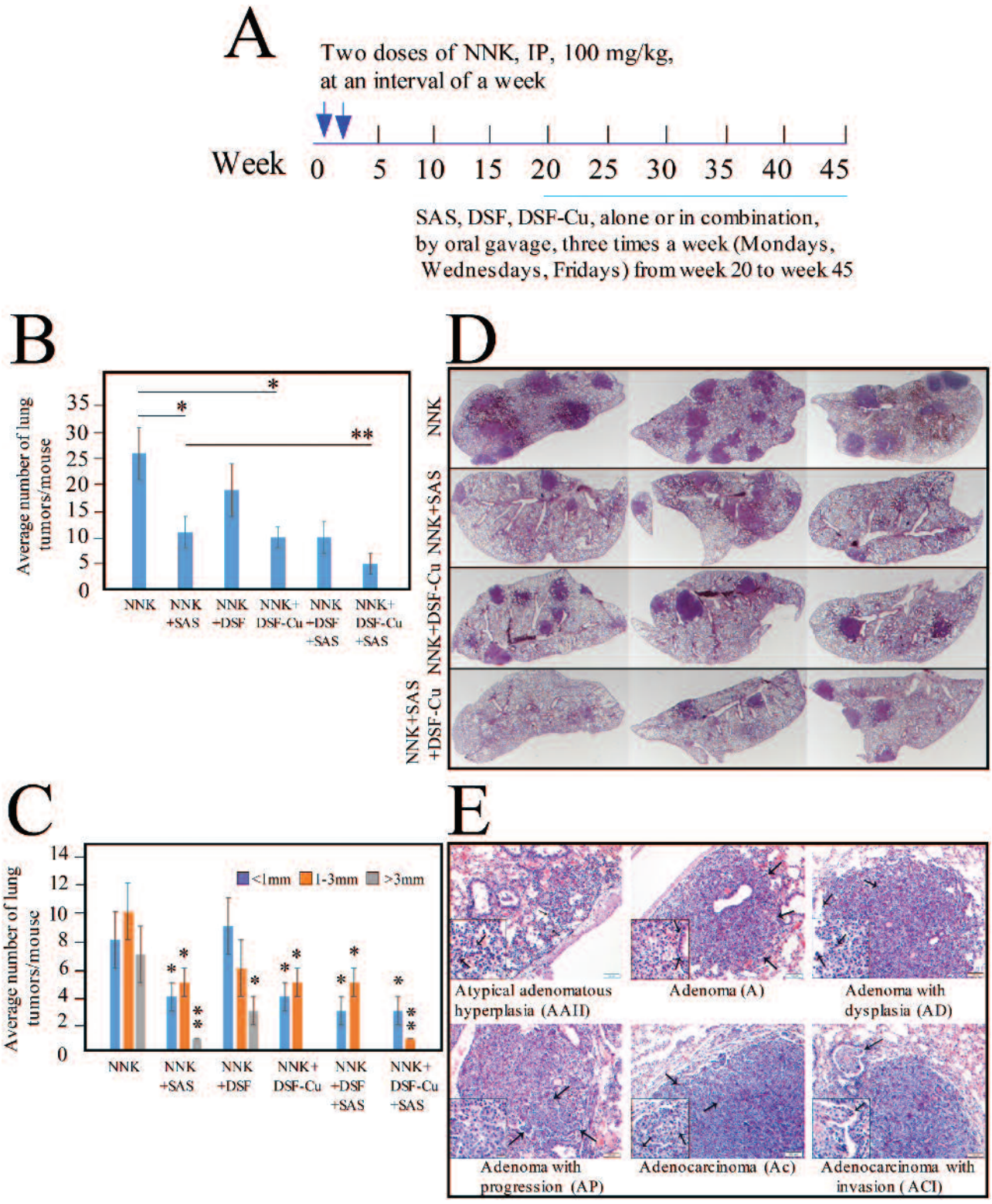

Figure 5. SAS and/or DSF-Cu inhibited lung adenocarcinoma formation in A/J mice. (**A**) Experimental design of the study. Mice (15 mice/group) were assigned to NNK control, NNK + SAS, NNK + DSF, NNK + DSF-CU, NNK + SAS + DSF or NNK + SAS + DSF-Cu groups, treated with two doses of NNK (100 mg/kg body weight, ip injection), at an interval of a week, and beginning 20 weeks after the first NNK dose, received, via oral gavage, vehicle or SAS and/or DSF/DSF-Cu, three times a week, until the end of the study at week 45. Effects of SAS and/or DSF-Cu on multiplicities of tumors on the surface of the lung (**B**) and size of tumors (**C**) as determined by analysis of the number and size of lung tumors immediately after the sacrifice of the mice (15 mice/group). (**D**) Representative images showing the number and size of lung tumors in tissue sections prepared from the lungs of different groups of mice. (**E**) Representative images of the different classes of NNK-induced microscopic lesions. *$P < 0.05$; **$P < 0.01$ indicate differences between NNK versus NNK + SAS, NNK + DSF or NNK + DSF-Cu or NNK + SAS versus NNK + SAS + DSF or NNK + SAS + DSF-Cu.

Table 1. Effects of SAS and DSF-Cu, alone or in combination, on multiplicities and incidence of NNK-induced histopathological lung lesions

Treatment	Histopathological lesions									
	Atypical adenomatous hyperplasia (AAH)		Adenoma (A)		Adenoma with dysplasia (AD)		Adenoma with progression (AP)		Adenocarcinoma (Ac)	
	Tumors/ mouse (mean ± SD)	Incidence (%)	Tumors/ mouse (mean ± SD)	Incidence (%)	Tumors/ mouse (mean ± SD)	Incidence (%)	Tumors/ mouse (mean ± SD)	Incidence (%)	Tumors/ mouse (mean ± SD)	Incidence (%)
NNK	5.2 ± 3.3	100	2.6 ± 2.3	80	5.0 ± 2.6	100	3.2 ± 3.3	80	4.0 ± 2.2	100
NNK + DSF-Cu	3.4 ± 2.5	100	2.4 ± 1.9	80	2.8 ± 1.9	100	2.6 ± 3.6	80	1.4 ± 1.1*	80
NNK + SAS	4.0 ± 3.2	100	0.8 ± 0.8	60	1.8 ± 2.9	60	1.6 ± 2.6	40	1.6 ± 2.3	40
NNK + DSF-Cu + SAS	1.8 ± 1.8	60	1.8 ± 1.5	80	4.0 ± 4.7	60	2.2 ± 2.5	60	0.8 ± 1.3*	40

*$P < 0.05$ compared with the control (NNK) group.

also minimizing any adverse effects and decreasing dosage at an equal or increased level of efficacy (40). In the present study, we showed that combinations of low concentrations of SAS and DSF-Cu reduced the viability of NSCLC cells by about 64–88%, compared with 20–40% reduction by the individual drugs, clearly indicating the benefits of combinatory treatment approach in terms of higher anticancer efficacy at concentrations that are therapeutically achievable. The observed resistance of NSCLC cells to therapeutically achievable concentrations of SAS are possibly due to overexpression of NRF2 and its effectors xCT and ALDH1A1 which could compensate and maintain redox homeostasis and mitigate cell death. In support of this, abrogation of SAS-induced NRF2, xCT and ALDH1A1 by low concentrations of DSF-Cu enhanced oxidative stress and potentiated the apoptotic effects of SAS. In line with our findings, NRF2 has been shown to account for the resistance of ovarian cancer cells to erastin, a drug which, like SAS, inhibits xCT, prevents GSH synthesis and ultimately causes cell death, and inhibition of NRF2 sensitized cells to erastin (41). Likewise, head and neck squamous cell carcinoma cells have been found to develop resistance to SAS, erastin as well as to buthionine sulfoximine, an inhibitor of GSH synthesis, via overexpression of ALDH3A1 and pharmacological or siRNA-mediated targeting ALDH3A1 markedly reduced the survival of the resistant cells (42).

Our present findings as well as several literature reports (16–20) have shown that DSF-Cu, but not DSF or Cu alone, exhibited a stronger anticancer activity, probably due to the complex formed by diethyldithiocarbamate (DTC), DSF's reactive metabolite and Cu, which plays a crucial role in redox reactions and generation of ROS (43). Also, DTC-Cu accumulated in tumor tissues at a level about an order of magnitude higher than the amount in normal tissues from the same animals and this preferential accumulation of DTC-Cu in tumors was ascribed to the higher levels of Cu (2- to 3-fold) in tumor cells (18). The possible differential accumulation of DSF-Cu in A549 and H2030 cells and the resulting marked ROS burst could have played a key role for the stronger apoptotic effects of DSF-Cu in A549 and H2030 cells and in reversing the resistance of these cells to SAS. Other mechanisms, including inhibition of NF-κB, the proteasome or ALDH (44) may also be involved in the observed anticancer effects of DSF-Cu. However, the free radical scavenger *N*-acetyl-cysteine has been shown to abrogate apoptosis induced by DSF-Cu (20), suggesting that the main mechanism for the anticancer effects of DSF-Cu is ROS generation.

In the A/J mouse-NNK model of lung tumor, lung adenoma arises around week 20 from foci of hyperplasia, whereas adenocarcinomas develop from adenomas progressing through adenoma with dysplasia and adenoma with progression, with continuing cell proliferation accompanied by mutations and karyotypic instability (32,45). Although several dietary and pharmaceutical agents have been found to suppress the development of pulmonary hyperplastic lesions into lung adenoma, only a few agents have been tested for their efficacy to inhibit lung adenocarcinoma, the most critical stage during the development of lung cancer (46). In the present study, mice treated with SAS or DSF-Cu alone exhibited significantly fewer and smaller tumors, compared with the control group, but combination of SAS and DSF-Cu was more effective in reducing the number and size of NNK-induced lung tumors. These effects are interesting as large tumors could be mainly adenocarcinomas and pose a greater risk to lung cancer patients compared with small, slow-growing tumors that may remain latent for long periods (47). Indeed, histopathology studies revealed that SAS and DSF-Cu, alone or in combination, suppressed malignant progression of preneoplastic lesions resulting in fewer lung adenocarcinoma. However, the multiplicity of lung adenoma was not significantly reduced. This may be because only a few adenomas having highly proliferating cells are sensitive to the drugs. In line with this, a previous study (48), demonstrated that only a small number of adenomas, about 14%, induced by tobacco smoke carcinogens actually progressed to malignancy.

In summary, in light of the evidence presented here, combination of SAS and DSF-Cu is a promising preventive/therapeutic approach against lung adenocarcinoma. Despite the promising antilung tumor effects of SAS and DSF, both drugs have been shown to exhibit poor stability in the acidic environment and blood circulation, rapid metabolism and early clearance from systemic circulation, which remains as a challenge for clinical use of the drugs as an anticancer agent. One promising approach to improve cancer cell targeting by SAS

and DSF is nano-formulation (38), which is currently undergoing in our lab.

Supplementary material

Supplementary data are available at *Carcinogenesis* online.

Supplementary Figure 1. The 3D δ-score synergy map for the interaction between SAS and DSF-Cu generated using SynergyFinder 2.0 from MTT assay data based on the Bliss independence.

Supplementary Figure 2. Apoptosis induction in H2030 cells treated with SAS and/or DSF/DSF-Cu alone or in combination for 48 h as determined by flow cytometry-based annexin V/propidium iodide assay. Bar graphs show mean ± SD of the percentage of apoptotic cells from three assays. $^{**}P < 0.01$; $^{***}P < 0.00$, compared with untreated cells.

Supplementary Figure 3. Bar graphs showing the mean ± SD expression of different proteins shown in Figure 4 as determined by western immunoblotting assays in three independent assays. Densitometry measurements of western blot bands were performed using digitalized scientific software program UN-SCAN-IT software. $^{*}P < 0.05$; $^{**}P < 0.01$; $^{***}P < 0.001$ compared with the control group.

Supplementary Figure 4. Full-length western immunoblots for the proteins analyzed in Figure 4. All indicated proteins were analyzed from the same gel and cropping area was indicated by black-lined rectangle in the full western immunoblot. In order to identify several proteins simultaneously, western blot membranes were cut at areas corresponding the molecular weight of the protein of interest.

Funding

This study was supported by NIH/NCI grant (R01 CA231210-01A1) to F.K.

Acknowledgement

Conflict of Interest Statement: None declared.

Data availability

The data underlying this article will be shared on reasonable request to the corresponding author.

References

1. Siegel, R.L. et al. (2022) Cancer statistics, 2022. *CA Cancer J. Clin.*, 72, 7–33.
2. Simanshu, D.K. et al. (2017) RAS proteins and their regulators in human disease. *Cell*, 170, 17–33.
3. Weinberg, F. et al. (2010) Mitochondrial metabolism and ROS generation are essential for Kras-mediated tumorigenicity. *Proc. Natl. Acad. Sci. USA*, 107, 8788–8793.
4. DeNicola, G.M. et al. (2011) Oncogene-induced Nrf2 transcription promotes ROS detoxification and tumorigenesis. *Nature*, 475, 106–109.
5. Lim, J.K.M. et al. (2019) Cystine/glutamate antiporter xCT (SLC7A11) facilitates oncogenic RAS transformation by preserving intracellular redox balance. *Proc. Natl. Acad. Sci. USA*, 116, 9433–9442.
6. Koppula, P. et al. (2018) Amino acid transporter SLC7A11/xCT at the crossroads of regulating redox homeostasis and nutrient dependency of cancer. *Cancer Commun. (Lond.)*, 38, 12.
7. Ji, X. et al. (2018) xCT (SLC7A11)-mediated metabolic reprogramming promotes non-small cell lung cancer progression. *Oncogene*, 37, 5007–5019.
8. Ishimoto, T. et al. (2011) CD44 variant regulates redox status in cancer cells by stabilizing the xCT subunit of system xc(–) and thereby promotes tumor growth. *Cancer Cell*, 19, 387–400.
9. Hu, K. et al. (2020) Suppression of the SLC7A11/glutathione axis causes synthetic lethality in KRAS-mutant lung adenocarcinoma. *J. Clin. Invest.*, 130, 1752–1766.
10. Yoshikawa, M. et al. (2013) xCT inhibition depletes CD44v-expressing tumor cells that are resistant to EGFR-targeted therapy in head and neck squamous cell carcinoma. *Cancer Res.*, 73, 1855–1866.
11. Otsubo, K. et al. (2017) Phase I study of salazosulfapyridine in combination with cisplatin and pemetrexed for advanced non-small-cell lung cancer. *Cancer Sci.*, 108, 1843–1849.
12. Shitara, K. et al. (2017) Dose-escalation study for the targeting of CD44v+ cancer stem cells by sulfasalazine in patients with advanced gastric cancer (EPOC1205). *Gastric Cancer*, 20, 341–349.
13. Robe, P.A. et al. (2018) Early termination of ISRCTN45828668, a phase ½ prospective, randomized study of sulfasalazine for the treatment of progressing malignant gliomas in adults. *BMC Cancer*, 9, 372.
14. Kim, J.Y. et al. (2009) Sulfasalazine induces haem oxygenase-1 via ROS-dependent Nrf2 signaling, leading to control of neointimal hyperplasia. *Cardiovasc. Res.*, 82, 550–560.
15. Rojo de la Vega, M. et al. (2018) NRF2 and the hallmarks of cancer. *Cancer Cell*, 34, 21–43.
16. Zhang, H. et al. (2010) Disulfiram treatment facilitates phosphoinositide 3-kinase inhibition in human breast cancer cells in vitro and in vivo. *Cancer Res.*, 70, 3996–4004.
17. Chen, D. et al. (2006) Disulfiram, a clinically used anti-alcoholism drug and copper-binding agent, induces apoptotic cell death in breast cancer cultures and xenografts via inhibition of the proteasome activity. *Cancer Res.*, 66, 10425–10433.
18. Skrott, Z. et al. (2017) Alcohol-abuse drug disulfiram targets cancer via p97 segregase adaptor NPL4. *Nature*, 552, 194–199.
19. Zha, J. et al. (2014) Disulfiram targeting lymphoid malignant cell lines via ROS-JNK activation as well as Nrf2 and NF-kB pathway inhibition. *Transl. Med.*, 12, 163.
20. Xu, B. et al. (2017) Disulfiram/copper selectively eradicates AML leukemia stem cells in vitro and in vivo by simultaneous induction of ROS-JNK and inhibition of NF-κB and Nrf2. *Cell Death Dis.*, 8, e2797.
21. IARC Working Group on the Evaluation of Carcinogenic Risks to Humans (2012) Personal habits and indoor combustions. Volume 100 E. A review of human carcinogens. *IARC Monogr. Eval. Carcinogen. Risks Hum.*, 100, 1–538.
22. Keohavong, P. et al. (2011) K-ras mutations in lung tumors from NNK-treated mice with lipopolysaccharide-elicited lung inflammation. *Anticancer Res.*, 31, 2877–2882.
23. Lei, H.M. et al. (2019) Aldehyde dehydrogenase 1A1 confers erlotinib resistance via facilitating the reactive oxygen species-reactive carbonyl species metabolic pathway in lung adenocarcinomas. *Theranostics*, 9, 7122–7139.
24. Ianevski, A. et al. (2022) SynergyFinder 3.0: an interactive analysis and consensus interpretation of multidrug synergies across multiple samples. *Nucleic Acids Res.*, 50, W739–W743.
25. Song, J.M. et al. (2017) Triptolide suppresses the in vitro and in vivo growth of lung cancer cells by targeting hyaluronan-CD44/RHAMM signaling. *Oncotarget*, 8, 26927–26940.
26. Kassie, F. et al. (2022) Combinatory lung tumor inhibition by myo-inositol and iloprost/rapamycin: association with immunomodulation. *Carcinogenesis*, 43, 547–556.
27. Thanee, M. et al. (2021) Sulfasalazine modifies metabolic profiles and enhances cisplatin chemosensitivity on cholangiocarcinoma cells in in vitro and in vivo models. *Cancer Metab.*, 9, 11.

28. Lun, X. et al. (2017) Disulfiram when combined with copper enhances the therapeutic effects of temozolomide for the treatment of glioblastoma. *Clin. Cancer Res.*, 22, 3860–3875.
29. Reagan-Shaw, S. et al. (2008) Dose translation from animal to human studies revisited. *FASEB J.*, 22, 659–661.
30. Huang, J. et al. (2016) A phase I study to repurpose disulfiram in combination with temozolomide to treat newly diagnosed glioblastoma after chemoradiotherapy. *J. Neurooncol.*, 128, 259–266.
31. Uauy, R. et al. (2008) Estimating risk from copper excess in human populations. *Am. J. Clin. Nutr.*, 88, 867S–871S.
32. Dagne, A. et al. (2011) Enhanced inhibition of lung adenocarcinoma by combinatorial treatment with indole-3-carbinol and silibinin in A/J mice. *Carcinogenesis*, 32, 561–567.
33. Nikitin, A.Y. et al. (2004) Classification of proliferative pulmonary lesions of the mouse: recommendations of the mouse models of human cancers consortium. *Cancer Res.*, 64, 2307–2316.
34. Redza-Dutordoir, M. et al. (2016) Activation of apoptosis signaling pathways by reactive oxygen species. *Biochim. Biophys. Acta*, 1863, 2977–2992.
35. Sauer, H. et al. (2001) Reactive oxygen species as intracellular messengers during cell growth and differentiation. *Cell. Physiol. Biochem.*, 11, 173–186.
36. Frantzi, M. et al. (2020) Drug repurposing in oncology. *Lancet Oncol.*, 21, e543.
37. Guastavino, E. et al. (1988) Ulcerative colitis in children. Levels of salicylazosulfapyridine and sulfapyridine during treatment [Spanish]. *Acta Gastroenterol. Latinoam.*, 18:107–113.
38. Farooq, M.A. et al. (2019) Recent advances in the delivery of disulfiram: a critical analysis of promising approaches to improve its pharmacokinetic profile and anticancer efficacy. *Daru*, 27, 853–862.
39. Zaher, H. et al. (2006) Breast cancer resistance protein (Bcrp/abcg2) is a major determinant of sulfasalazine absorption and elimination in the mouse. *Mol. Pharm.*, 3, 55–61.
40. Rizeq, B. et al. (2020) The Power of phytochemicals combination in cancer chemoprevention. *J. Cancer*, 11, 4521–4533.
41. Liu, N. et al. (2020) Activation of the reverse transsulfuration pathway through NRF2/CBS confers erastin-induced ferroptosis resistance. *Br. J. Cancer*, 122, 279–292.
42. Okazaki, S. et al. (2018) Synthetic lethality of the ALDH3A1 inhibitor dyclonine and xCT inhibitors in glutathione deficiency-resistant cancer cells. *Oncotarget*, 9, 33832–33843.
43. Jiang, Y. et al. (2022) Copper-induced tumor cell death mechanisms and antitumor theragnostic applications of copper complexes. *Nanomedicine (Lond.)*, 17, 303–324.
44. Kannappan, V. et al. (2021) Recent advances in repurposing disulfiram and disulfiram derivatives as copper-dependent anticancer agents. *Front Mol. Biosci.*, 8, 741316.
45. Belinsky, S.A. et al. (1992) Role of the alveolar type II cell in the development and progression of pulmonary tumors induced by 4-(methylnitrosamino)-1-(3-pyridyl)-1-butanone in the A/J mouse. *Cancer Res.*, 52, 3163–3173.
46. Keith, R.L. et al. (2013) Lung cancer chemoprevention: current status and future prospects. *Nat. Rev. Clin. Oncol.*, 10, 334–343.
47. Garbow, J.R. et al. (2008) Quantitative monitoring of adenocarcinoma development in rodents by magnetic resonance imaging. *Clin. Cancer Res.*, 14, 1363–1367.
48. Conaway, C.C. et al. (2005) Phenethyl isothiocyanate and sulforaphane and their N-acetylcysteine conjugates inhibit malignant progression of lung adenomas induced by tobacco carcinogens in A/J mice. *Cancer Res.*, 65, 8548–8557.